Palaeogeography, Palaeoclimatology, Palaeoecology 692 (2026) 113755

Contents lists available at ScienceDirect

Palaeogeography, Palaeoclimatology, Palaeoecology

journal homepage: www.elsevier.com/locate/palaeo

Stable strontium isotopes of Late Devonian conodonts from Kowala (Poland) reveal genus-level signatures

Przemysław Lech Świś [a], Annalisa Ferretti [a,*], Manuel Rigo [b,c,*], Thomas Letulle [b], Anna Cipriani [a], Luca Medici [d], Daniele Malferrari [a], Federico Lugli [a]

[a] Department of Chemical and Geological Sciences, University of Modena and Reggio Emilia, via G. Campi 103, 41125 Modena, Italy
[b] Department of Geosciences, University of Padova, via G. Gradenigo 6, 35131 Padova, Italy
[c] IGG-CNR, via G. Gradenigo 6, 35131 Padova, Italy
[d] National Research Council of Italy, Institute of Methodologies for Environmental Analysis, C.da S. Loja-Zona Industriale, 85050 Tito Scalo, Potenza, Italy

ARTICLE INFO

Editor: B Shen

Keywords:
Bioapatite
Isotope fractionation
Diagenetic preservation
Trophic ecology
Physiological differentiation
Vital effects

ABSTRACT

Conodonts are extinct early vertebrates whose apatite oral elements provide one of the most extensive vertebrate fossil records widely used in biostratigraphy and paleoceanography. However, their trophic ecology and physiological differentiation remain poorly constrained. Here we investigate stable strontium isotope compositions ($\delta^{88}Sr$) in six conodont genera from a well-preserved latest Famennian (Upper Devonian) succession at the Kowala Quarry (Holy Cross Mountains, Poland), spanning three conodont biozones. After detailed assessment of diagenetic preservation using crystallographic, elemental, and radiogenic Sr isotope data ($^{87}Sr/^{86}Sr$), we show that conodont bioapatite retains a primary biological $\delta^{88}Sr$ signal. Statistically significant genus-level differences in $\delta^{88}Sr$ are observed and persist after correction for stratigraphic trends. The studied genera cluster into two distinct groups, with *Palmatolepis*, *Bispathodus*, and *Pandorinellina* showing higher $\delta^{88}Sr$ values than *Branmehla*, *Mehlina*, and *Idioprioniodus*. These differences are consistent with biologically driven isotope fractionation and likely reflect trophic niche differentiation and/or digestive physiology (vital effects) rather than diagenetic overprinting. Comparison with apparatus architecture indicates that $\delta^{88}Sr$ variations correlate most strongly with P_1 element morphology: taxa with blade-like P_1 elements display lower $\delta^{88}Sr$ values than those with platform-, icrion-, or expanded basal cavity morphologies. Our results demonstrate that stable Sr isotopes provide a novel proxy for reconstructing trophic structure and ecological differentiation in extinct marine vertebrate communities.

1. Introduction

Conodonts are an extinct group of small, lamprey-shaped early vertebrates that thrived in marine ecosystems for over 300 million years, from the late Cambrian to the Early Jurassic (Du et al., 2020, 2023; Ferretti et al., 2020). They were the first vertebrates to develop hard apatite dental tooth-like elements in an otherwise completely soft body organism (Murdock et al., 2013). The conodont feeding apparatus, with a few exceptions (Liu et al., 2017), typically comprised 15 to 19 elements arranged with clear bilateral symmetry. Although their crown tissues are not homologous to those of gnathostomes (Sansom et al., 1992), conodonts nonetheless record the early emergence of defining vertebrate features in marine environments and represent a key factor in the group's evolutionary success.

Conodont elements are among the most abundant vertebrate fossils in carbonate sediments (Foote and Sepkoski, 1999) and are widely used for detailed bio- and chrono-stratigraphic correlations (*e.g.*, Corradini et al., 1998; Schönlaub et al., 2017). This outstanding fossil record, coupled with their exceptionally high evolutionary rate, has made conodonts one of the most valuable tools in biostratigraphy, enabling the establishment of over 240 biozones across the entire Paleozoic and Triassic (Henderson, 2020). Conodonts are also the most frequently used index fossils for defining Global Stratigraphic Section and Points (GSSPs), with 27 GSSPs based on the first appearance datum (FAD) of conodont species (Corradini et al., 2026), and conodonts have also been proposed as primary markers in additional cases (*e.g.*, Krystyn, 2010; Rigo et al., 2016). Beyond stratigraphy, conodonts are also commonly used in geochemical reconstructions of past climate and ocean chemistry

* Corresponding authors.
E-mail addresses: ferretti@unimore.it (A. Ferretti), manuel.rigo@unipd.it (M. Rigo).

https://doi.org/10.1016/j.palaeo.2026.113755
Received 22 January 2026; Received in revised form 22 March 2026; Accepted 22 March 2026
Available online 24 March 2026

(*e.g.*, Joachimski and Buggisch, 2002; Rigo and Joachimski, 2010; Rigo et al., 2012; Trotter et al., 2015; Le Houedec et al., 2017).

Despite this prominence, conodont paleoecology remains difficult to constrain because conodonts are known almost exclusively from their oral elements. Nevertheless, important insights into conodont lifestyles have been obtained from oxygen isotopes of biogenic conodont apatite (*e.g.*, Rigo and Joachimski, 2010; Trotter et al., 2015; Du et al., 2021). More recently, a growing body of work combining geochemical proxies and morphological approaches supports ecological differentiation among taxa (see, among others, Shirley et al., 2018; Balter et al., 2019; Zhuravlev, 2020; Zhuravlev et al., 2020; Terrill et al., 2022), together with morphological investigations (Kelz et al., 2023; Assemat et al., 2023; Goudemez et al., 2026). For example, Terrill et al. (2022) showed that different conodont taxa preserve different Sr/Ca and Ba/Ca ratios, indicating likely variation in trophic partitioning. Balter et al. (2019) suggested that Devonian conodonts were possibly first level consumers, based on their calcium isotope ratio ($\delta^{44/42}Ca$).

Strontium isotopes provide complementary ways to explore both environmental context and biological differentiation. Radiogenic Sr ratios ($^{87}Sr/^{86}Sr$) have long been used to correlate marine carbonates and apatites because seawater $^{87}Sr/^{86}Sr$ evolution is relatively well constrained through time (*e.g.*, Veizer et al., 1999; Korte et al., 2003; Onoue et al., 2018; McArthur et al., 2020). More recently, stable Sr isotopes have been shown to fractionate in vertebrate hard tissues in relation to trophic niche partitioning and digestive physiology. These processes tend to favor incorporation of lighter isotopes (^{86}Sr) into bioapatite relative to heavier isotopes (^{88}Sr), thus bioapatite is often depleted in ^{88}Sr compared to the diet (*i.e.*, lower $^{88}Sr/^{86}Sr$ or $\delta^{88}Sr$ in ‰ against NIST-SRM987) (Knudson et al., 2010; Lewis et al., 2017; Guiserix et al., 2024; Armaroli et al., 2025; Michailow et al., 2025; Weber et al., 2025). Yet, the mechanisms underlying $\delta^{88}Sr$ variability in bioapatite remain poorly understood, and the relative influence of dietary, metabolic, and digestive physiological processes on these values in past vertebrates is still uncertain. To date, $\delta^{88}Sr$ values in conodonts through time have been reported only by Le Houedec et al. (2017), and ecological signals at the genus level remain largely unexplored.

Here, we determine the stable Sr isotope composition ($\delta^{88}Sr$) in six Late Devonian conodont genera to investigate possible differences in trophic ecology, habitat, and/or metabolic processes (*i.e.*, vital effects), after a thorough assessment of diagenetic preservation. Samples were collected from the 10 m-thick Kowala Quarry section in Poland, spanning the three latest Famennian conodont biozones. The analysed material derives from exceptionally preserved collections with a low 1.5 CAI - Colour Alteration Index (Epstein et al., 1977). Genera were specifically selected to represent diverse apparatus morphologies as well as different types of P_1 element, the most distinctive and diagnostic element.

2. Geological setting

The material investigated comes from the upper Famennian interval of the Kowala Quarry in the Holy Cross Mountains (central Poland) (Fig. 1). The active quarry lies on the southern limb of the Gałęzice-Bolechowice Syncline and exposes a continuous marine succession of marly limestones and shales deposited in the Chęciny-Zbrza intrashelf basin. The section documents a drowned, low-oxygen shelf setting adjacent to a shallower pelagic ridge to the south (Racki, 1993).

The material examined in this study originates from a well-defined stratigraphic interval within the Upper Devonian succession of the Kowala section, spanning from approximately 1.5 m below the Kowala Black Shale (KBS) to the Hangenberg Black Shale (HBS) (Fig. 1C). This interval encompasses the transition from the late Famennian into the earliest Carboniferous, a critical period marked by significant paleoenvironmental changes and biotic turnovers (see, *e.g.*, House, 2002; Becker et al., 2016; Kaiser et al., 2016). Lithologically, the interval consists of rhythmically interbedded marly limestones and shales of the Wocklumeria Limestone (informal unit L; Szulczewski and Skompski, 1995; De Vleeschouwer et al., 2013). The beds record deposition under fluctuating redox conditions with repeated incursions of anoxia. The upper part of the unit contains several thin ash beds and tuffites, linked to volcanism in the Pripyat-Dnieper-Donets-Donbas rift system (Pisarzowska et al., 2022). These volcaniclastic layers provide additional valuable chronostratigraphic markers and constrain the age of the Hangenberg Black Shale to approximately 359 Ma (Myrow et al., 2014).

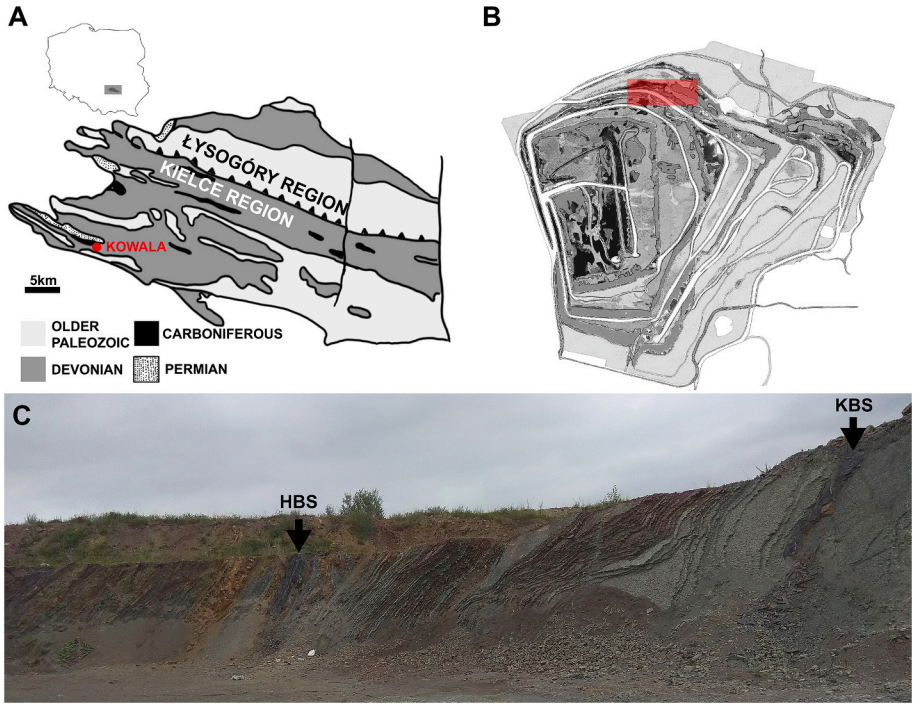

Fig. 1. (A) Map of the Holy Cross Mountains showing the location of the Kowala Quarry. (B) Simplified satellite image of the quarry with the sampling site indicated. (C) Photograph of the studied section. HBS = Hangenberg Black Shale; KBS = Kowala Black Shale.

The KBS represents a regionally developed, organic-rich horizon marking an anoxic episode confined to the Chęciny-Zbrza basin (De Vleeschouwer et al., 2013), while the HBS corresponds to the globally recognised Hangenberg Event, one of the most significant environmental crises of the late Paleozoic (see, among others, Marynowski et al., 2012; Pisarzowska et al., 2020).

Biostratigraphic calibration follows the conodont zonation of Kaiser (2009) and Becker et al. (2016, 2020, 2021), based on previous conodont investigations conducted on this location (Malec, 2014; Matyja et al., 2021; Dzik et al., 2022). The succession begins in the *Bispathodus costatus* Zone, with *B. ultimus* first appearing below the KBS and *Siphonodella* (*Eosiphonodella*) *praesulcata* occurring 2.9 m above its base, defining the *B. ultimus* and *S.* (*E.*) *praesulcata* zones, respectively. Conodonts are absent within the HBS itself, but the last occurrences of *B. costatus* and *B. ultimus* at its base mark the *Bispathodus costatus-Protognathodus kockeli* Interregnum. *Protognathidus kockeli*, the marker species of the final Famennian zone, appears about 2 m above the HBS base (Matyja et al., 2021), immediately preceding the earliest Carboniferous *S.* (*E.*) *sulcata-P. kuehni* Zone, which is not documented in Kowala.

3. Material

The analysed material derives from exceptionally preserved collections with a low 1.5 CAI (Colour Alteration Index; Epstein et al., 1977). Genera were specifically selected to represent diverse apparatus morphologies as well as different types of P1 element, the most distinctive and diagnostic element. The elements analysed in this study belong primarily to the three most common latest Devonian genera: *Palmatolepis*, *Bispathodus*, and *Branmehla*. As noted previously, our analysis focused on P_1 elements, which display a wide range of morphological variation, including differences in platform outline, denticulation patterns, and basal cavity development. These three genera represent distinct types of molarization in the P_1 elements (Fig. 2). In *Palmatolepis*, ontogenetic growth produces a relatively broad surface extending beyond the main denticle row (carina), forming a platform; accordingly, *Palmatolepis* is considered a platform-bearing genus (Dzik, 2008). *Bispathodus* exhibits molarization through the multiplication of denticles along the carina, expanding and thickening the occlusal surface into an icrion (Dzik, 2006), and thus represents an icrion-bearing taxon. In contrast, *Branmehla* possesses a simple P_1 morphology in which the working surface comprises only the carina, characterising it as a blade-like element type (Dzik, 2006).

In addition, blade-like *Mehlina*, *Pandorinellina*, and *Idioprioniodus* from beds Ko-276 and Ko-409 were included in the analysis. Like *Branmehla*, these genera also possess blade-like P_1 elements, but they differ in basal cavity development. *Pandorinellina* has a relatively broad basal cavity, more comparable to that of *Bispathodus*. *Mehlina* and *Idioprioniodus*, on the other hand, exhibit very narrow basal cavities that are almost invisible in oral view. *Idioprioniodus* further differs by possessing notably more robust denticles. These additional taxa were included to incorporate variability in apparatus construction, which may influence feeding behaviour.

The ozarkodinid oral apparatus comprises fifteen elements arranged in three arrays: the rostralmost M elements, the intermediate S elements, and the pharyngeal P elements (Purnell et al., 2000). As mentioned above, the apparatus is bilaterally symmetrical, with most elements occurring as mirrored pairs. Only the M elements form a single pair and have been interpreted as grasping elements. The S-series includes four pairs plus the unpaired S_0. The P-series includes two pairs (P_2 and P_1), the latter being the most taxonomically diagnostic element. Apparatus reconstructions utilised in this study follow the hypothetico-deductive approach (Dzik, 1991) as applied in previous works (*e.g.*, van den Boogaard and Kuhry, 1979; Dzik, 2006). All taxa considered exhibit broadly similar apparatus layouts (Figs. 3 and 4), although they differ in the details of individual element morphology.

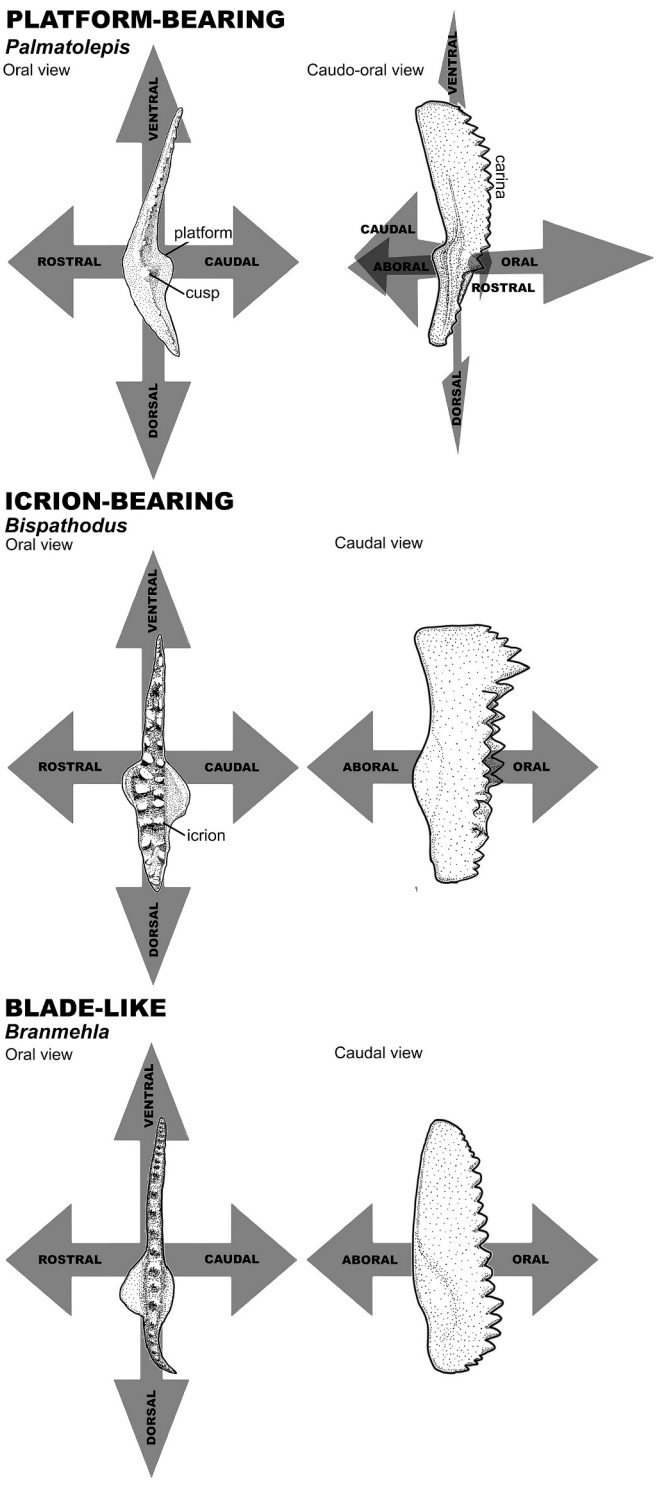

Fig. 2. Oral and caudal (caudalo-oral in *Palmatolepis*) views of the P_1 elements of the three primary Late Devonian genera studied herein *Palmatolepis*, *Bispathodus* and *Branmehla*, representing three distinct morphological types. Anatomical notation based on Purnell et al. (2000).

Palmatolepis has the most distinctive apparatus, with elongated anterior and posterior processes on the M elements, slender "spiky" S-series elements, and a uniquely triramous P_2. *Bispathodus* and *Pandorinellina* share the most similar apparatus configurations among the taxa studied, differing mainly in the robustness and density of denticulation, which is reflected in referring to *Pandorinellina vulgaris* as a morph inside *Bispathodus stabilis* species by some authors. *Mehlina* is broadly

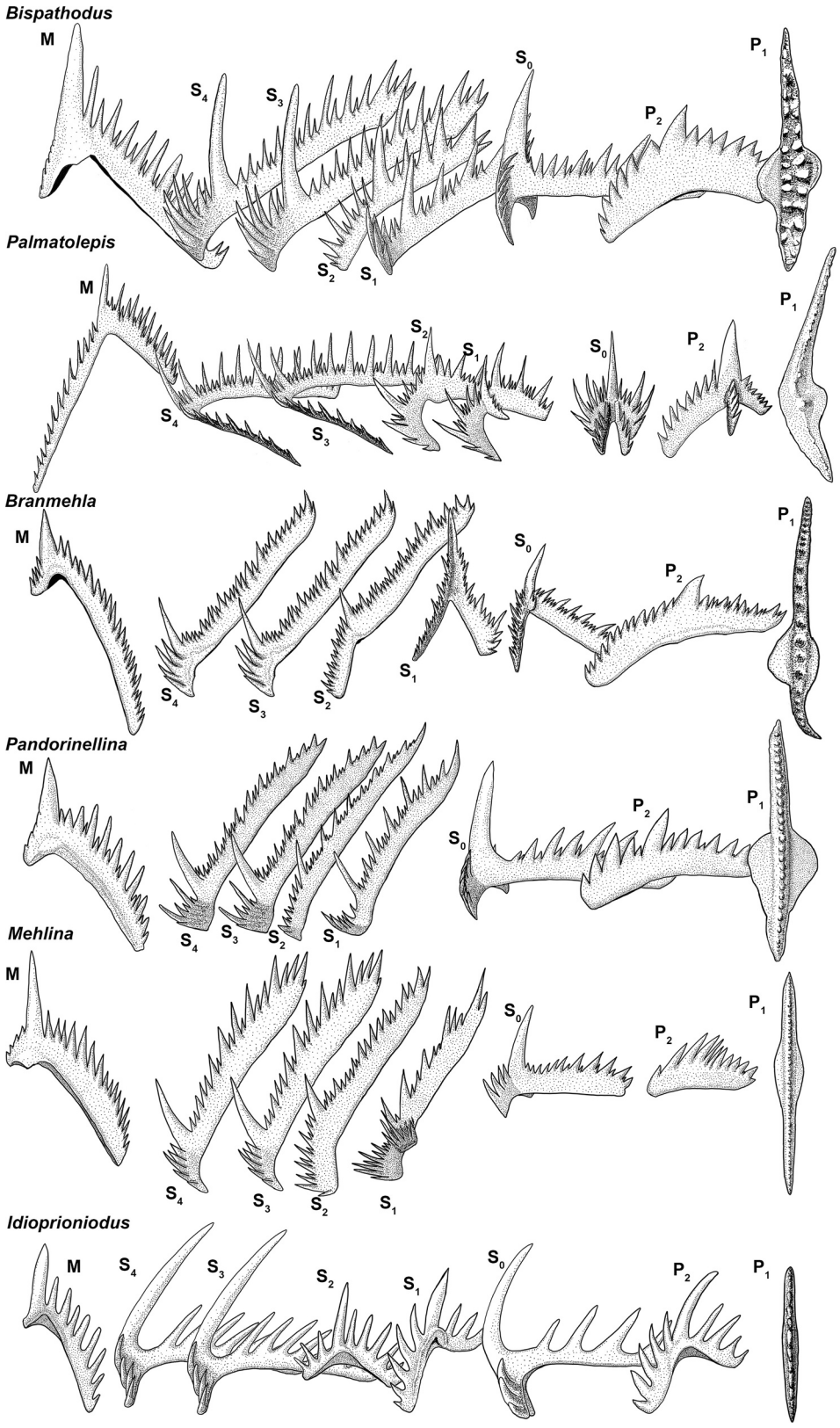

Fig. 3. Apparatus composition of the six Late Devonian genera studied in this paper.

comparable to these genera but has an additional process on the S_1 element and a shorter P_2. *Branmehla* is characterised by a distinctive triangular S_1 element. Finally, *Idioprioniodus* possesses a robust apparatus with thick, widely spaced denticles, and some of its elements exhibit unusually everted basal cavities (Dzik, 2006).

By examining these six genera that represent a mosaic of morphological traits, we aim to assess whether these traits correlate with conodont $\delta^{88}Sr$ values and, by extension, whether they reflect differences in feeding strategies.

The conodont collections are now deposited in the "Inventario

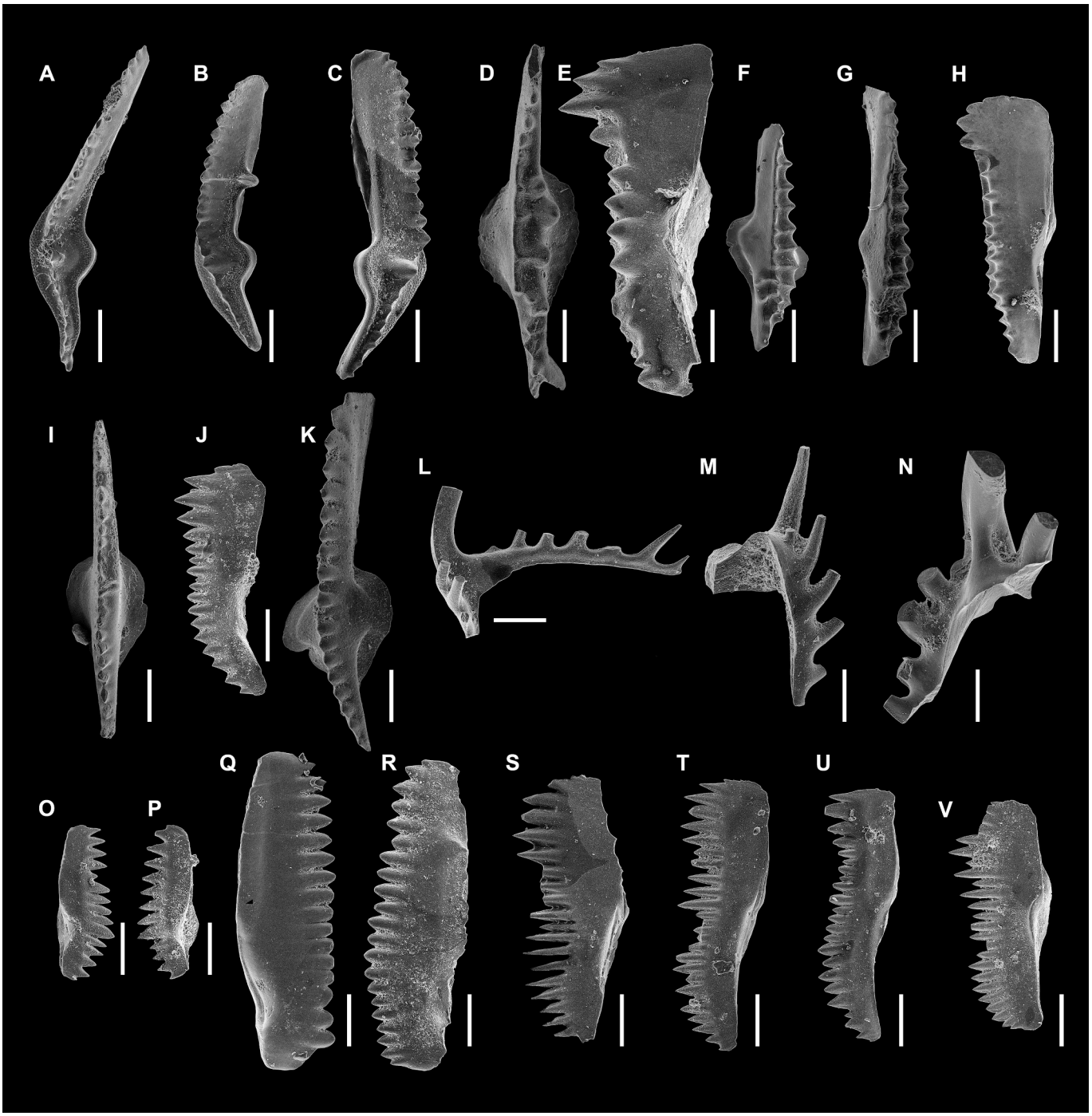

Fig. 4. Selected conodont elements analysed in this study. All P_1 elements (except *Idioprioniodus*). A-C: *Palmatolepis gracilis*; A: oral view of specimen IPUM 35246, sample Ko-281, *Siphonodella* (*Eosiphonodella*) *praesulcata* conodont Zone; B: oral view of specimen IPUM 35247, sample Ko-281, *S.* (*E.*) *praesulcata* conodont Zone; C: caudo-oral view of specimen IPUM 35248, sample Ko-281, *S.* (*E.*) *praesulcata* conodont Zone. D-E: *Bispathodus aculeatus*; D: oral view of specimen IPUM 35249, sample Ko-281, *S.* (*E.*) *praesulcata* conodont Zone; E: caudal view of specimen IPUM 35250, sample Ko-281, *S.* (*E.*) *praesulcata* conodont Zone. F: *Bispathodus spinulicostatus*: oral view of specimen IPUM 35251, sample Ko-281, *S.* (*E.*) *praesulcata* conodont Zone; G-H: *Bispathodus aculeatus*; G: oral view of specimen IPUM 35252, sample Ko-404, *Bispathodus ultimus* conodont Zone; H: caudal view of specimen IPUM 35253, sample Ko-404, *B. ultimus* conodont Zone. I-K: *Pandorinellina vulgaris*; I: oral view of specimen IPUM 35254, sample Ko-404, *B. ultimus* conodont Zone; J: caudal view of specimen IPUM 35255, sample Ko-276, *S.* (*E.*) *praesulcata* conodont Zone; K: oral view of specimen IPUM 35256, sample Ko-276, *S.* (*E.*) *praesulcata* conodont Zone. L-N: *Idioprioniodus ruptus*; L: caudo-dorsal view of $S_{3–4}$ element of specimen IPUM 35257, sample Ko-281, *S.* (*E.*) *praesulcata* conodont Zone; M: caudal view of S_1 element of specimen IPUM 35258, sample Ko-404, *B. ultimus* conodont Zone; N: caudal view of P_2 element of specimen IPUM 35259, sample Ko-404, *B. ultimus* conodont Zone. O-P: *Branmehla inornata*; O: caudal view of specimen IPUM 35260, sample Ko-404, *B. ultimus* conodont Zone; P: caudal view of specimen IPUM 35261, sample Ko-276, *S.* (*E.*) *praesulcata* conodont Zone. Q-R: *Branmehla suprema*; Q: caudal view of specimen IPUM 35262, sample Ko-281, *S.* (*E.*) *praesulcata* conodont Zone; R: caudal view of specimen IPUM 35263, sample Ko-276, *S.* (*E.*) *praesulcata* conodont Zone. S-W: *Mehlina strigosa*; S: caudal view of specimen IPUM 35264, sample Ko-281, *S.* (*E.*) *praesulcata* conodont Zone; T: caudal view of specimen IPUM 35265, sample Ko-404, *B. ultimus* conodont Zone; U: caudal view of specimen IPUM 35266, sample Ko-404, *B. ultimus* conodont Zone; V: caudal view of specimen IPUM 352676, sample Ko-404, *B. ultimus* conodont Zone.
Scale bars correspond to 200 μm.

Paleontologia Università di Modena e Reggio Emilia-IPUM" at the Department of Chemical and Geological Sciences, University of Modena and Reggio Emilia, Modena, Italy, under repository numbers IPUM 35246-35267.

4. Methods

Monogeneric samples of conodont elements were transferred to a clean plastic slide and inspected under a binocular microscope. When needed, a preliminary cleaning was performed under the binocular, using a soft-brush and 1 M acetic acid (suprapur®) to remove incrustings. Few elements were picked and weighted to reach a sample size of 150–200 μg. Elements were then fully cleaned with 0.5 M acetic acid (suprapur®) in an ultrasonic bath and rinsed with MilliQ water. Samples were finally dissolved in 0.5 ml of 3 M HNO_3 (suprapur®).

Strontium was purified by ion-exchange chromatography at the MeGic laboratory (https://www.geochem.unimore.it/) of the Department of Chemical and Geological Sciences (DSCG) of the University of Modena and Reggio Emilia (UNIMORE), Italy, following a modified version of the procedure described by Argentino et al. (2021), Armaroli et al. (2024), and Letulle et al. (2025). In-house teflon columns were packed with ~100 μl of Eichrom© Sr-spec resin, rinsed with 6 ml of Milli-Q water, and conditioned with 0.6 ml of 3 M HNO_3 prior to sample loading. After introducing the sample solution, the matrix was eluted and collected using 1.2 ml of 3 M HNO_3, while Sr retained on the resin was subsequently recovered with 6 ml of Milli-Q water. To ensure complete Sr recovery, the initial matrix eluate was reloaded onto the same column and processed again under identical conditions.

The $\delta^{88}Sr$ and $^{87}Sr/^{86}Sr$ ratios were determined simultaneously using a Neptune MC-ICPMS at the Centro Interdipartimentale Grandi Strumenti (CIGS) of UNIMORE, Italy, following Armaroli et al. (2025). Repeated analysis of NIST-SRM987 yielded an average $^{87}Sr/^{86}Sr$ ratio of 0.710265 ± 0.000017 (2SD, $n = 22$) and a reproducibility of ±0.05‰ (2SD, n = 22) for $\delta^{88}Sr$. NIST-SRM1400 (Bone Ash) was used as quality control reference material and processed along with the samples, yielding an average $^{87}Sr/^{86}Sr$ ratio of 0.71313 ± 0.00006 (2SD, $n = 23$) and a $\delta^{88}Sr$ value of −0.40‰ ± 0.10‰ (2SD, n = 23), in agreement with published values (Romaniello et al., 2015; Weber et al., 2018; Guiserix et al., 2022; Armaroli et al., 2024; Weber et al., 2025). All $^{87}Sr/^{86}Sr$ ratios were adjusted to a value of 0.710248 for NIST-SRM987 (McArthur et al., 2020). The typical in-run error (2SE) is ~0.00001 for $^{87}Sr/^{86}Sr$ and ~ 0.02‰ for $\delta^{88}Sr$.

Statistical analyses were conducted in R (version 4.0.5). The $\delta^{88}Sr$ and $^{87}Sr/^{86}Sr$ ratios were modeled using LOESS smoothing as a function (span = 0.75) of stratigraphic height to characterise baseline trends. Residuals ($\Delta^{88}Sr$ and $\Delta^{87}Sr/^{86}Sr$) from these LOESS models were then used to evaluate genus-level differences after removing stratigraphic trends. Due to the reduced sample sizes of some genera and the lack of homogeneity of variances, normality assumptions could not be met. Therefore, differences among genera were assessed using the non-parametric Kruskal-Wallis test. *Post hoc* pairwise comparisons were performed using Dunn's test with Holm correction for multiple testing. Statistical significance was set at $p < 0.05$.

To improve the diagenetic assessment of the specimens, we performed X-ray microdiffraction measurements on a subset of elements at the Institute of Methodologies for Environmental Analysis of the National Research Council of Italy of Tito Scalo (Potenza, Italy), following the protocol already tested by Ferretti et al. (2017, 2021, 2023), Malferrari et al. (2019, 2024) and Medici et al. (2020, 2021, 2026). The analysis was carried out on the mounted conodont elements of three genera (*Palmatolepis*, *Bispathodus*, *Branmehla*) from seven beds throughout all the section. Data were collected using a Rigaku D/MAX RAPID diffraction system, operating at 40 kV and 30 mA with a CuKα source (see Medici et al., 2020). X-ray microdiffraction was run on the denticles and the base ("planar surface" in Tables) of conodont elements. The analyses were carried out using the 0.1-mm collimator and with collection times of 2 h; after measurements, the unit-cell parameters (*a*, *c* and the cell volume) were refined using UnitCell software (Holland and Redfern, 1997).

On these specimens, microphotographs were collected and Ca/P (wt %) ratios and F (wt%) content were determined *via* ESEM-EDS at DSCG-UNIMORE. Reproducibility for Ca, P, and F was assessed using a modern shark tooth ($n = 5$ replicates) and yielded relative standard deviations (RSD; calculated as 100 * SD / mean) of 0.30%, 2.1%, and 16%, respectively. Carbon-coated selected specimens, mounted on aluminium stubs previously covered with carbon-conductive adhesive tape, were analysed using a JEOL JSM–6010PLUS/LA InTouchScope SEM equipped with an Energy-Dispersive X-ray (EDX) detector for elemental microanalyses. Measurements were performed in high vacuum with an accelerating voltage between 5 and 20 keV. Ten measurements were taken on the smooth and not-encrusted area of each element located near the basal cavity.

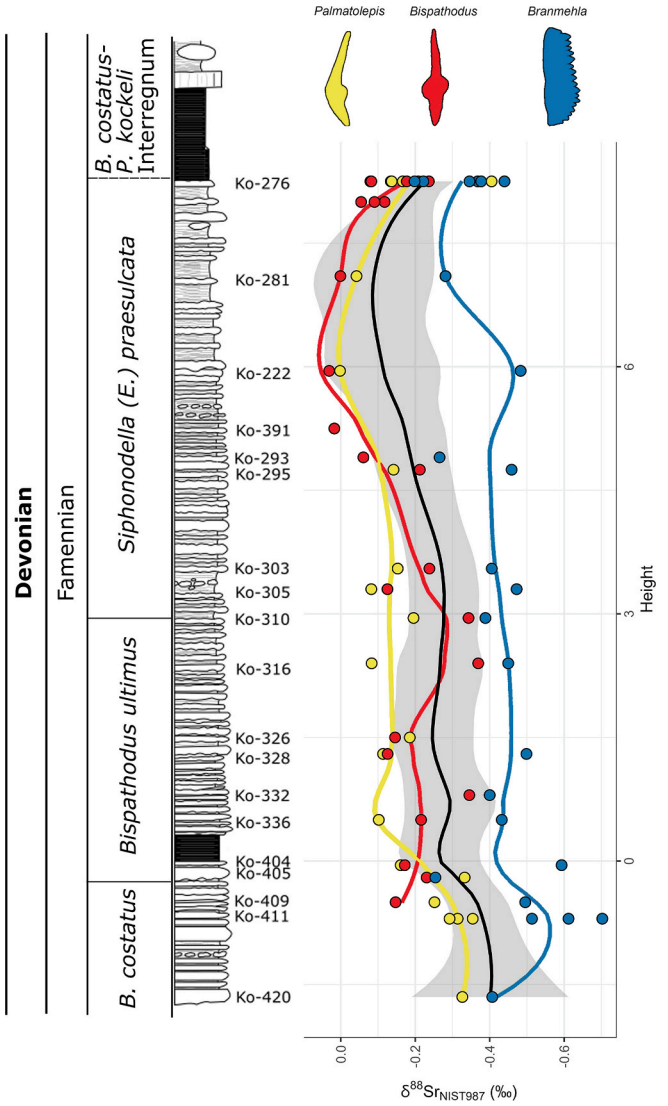

Fig. 5. $\delta^{88}Sr$ values of the three genera *Palmatolepis* (yellow, oral view), *Bispathodus* (red, oral view) and *Branmehla* (blue, caudal view) from the latest Devonian (Kowala Quarry) are reported against their section height. Colored lines are LOESS smoothing functions (span = 0.75). The black curve is the LOESS smoothing (span = 0.75) of the whole dataset, reported with a 95% confidence interval (grey band). Section log is based on Dzik et al. (2022); biostratigraphic zonation is based on Becker et al. (2020). (For interpretation of the references to colour in this figure legend, the reader is referred to the web version of this article.)

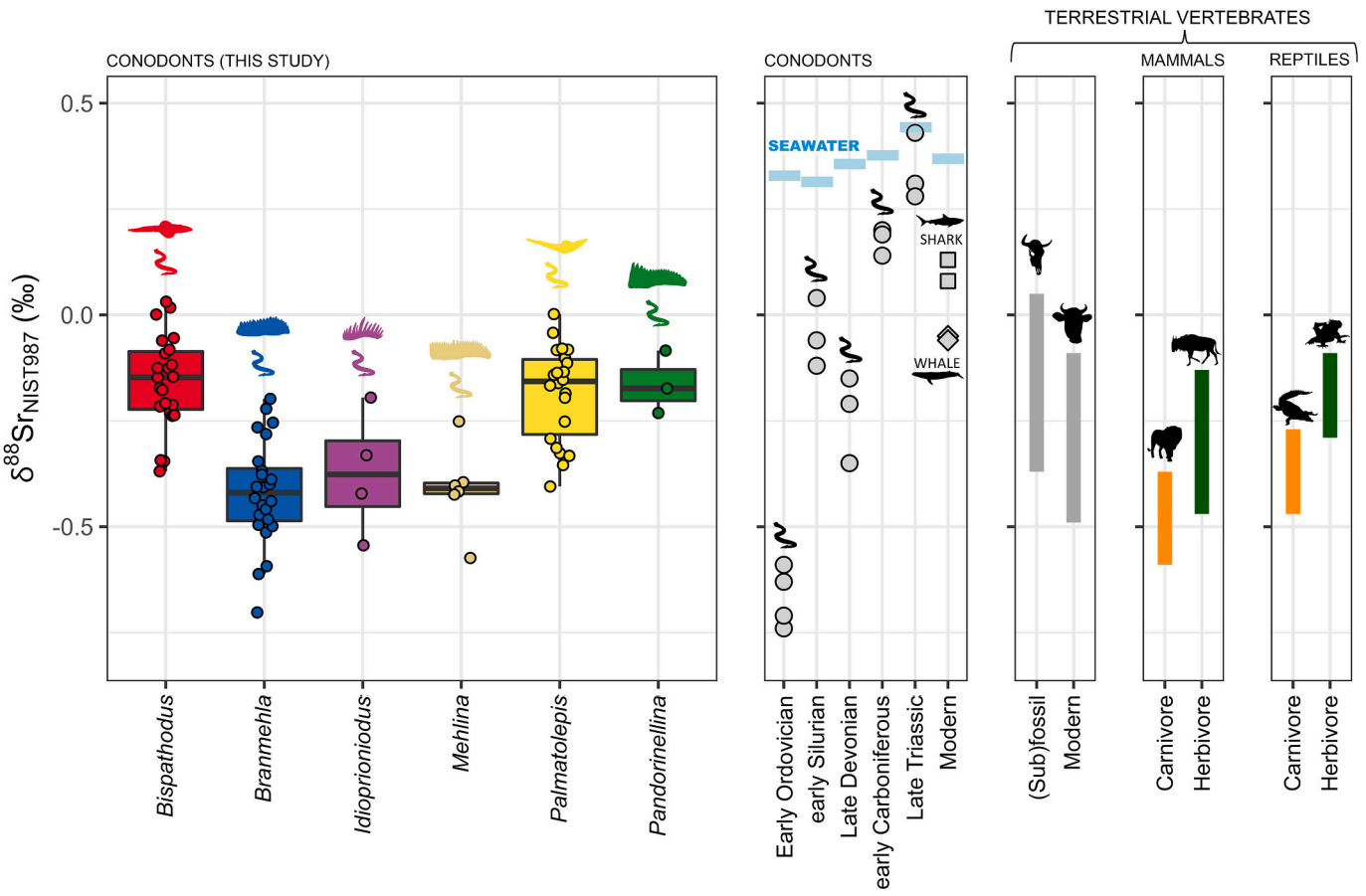

Fig. 6. $\delta^{88}Sr$ data of the six conodont genera investigated herein are reported along with conodont data from literature (Le Houedec et al., 2017), modern marine animals and terrestrial vertebrates (Tütken et al., 2015; Guiserix et al., 2022, 2024; Weber et al., 2025) with distinction between herbivores and carnivores. $\delta^{88}Sr$ values of seawater are calculated from brachiopods in Vollstaedt et al. (2014).

5. Results

The obtained $\delta^{88}Sr$ values (Figs. 5 and 6; Table SM-1) show statistical significant differences among the studied genera (Kruskal-Wallis rank sum $\chi^2 = 45.62$, $p = 1.1e\text{-}08$) and are consistent with previously reported values for Late Devonian conodonts (Le Houedec et al., 2017), as well as with bioapatite values from other (terrestrial) vertebrates (Tütken et al., 2015; Le Houedec et al., 2017; Guiserix et al., 2022, 2024; Armaroli et al., 2025; Weber et al., 2025). The average $\delta^{88}Sr$ values for the main genera *Palmatolepis*, *Bispathodus*, and *Branmehla* are −0.18‰ ± 0.11‰ (SD, $n = 22$), −0.16‰ ± 0.11‰ ($n = 23$), and − 0.42‰ ± 0.12‰ ($n = 24$), respectively. For *Mehlina*, *Idioprioniodus*, and *Pandorinellina*, the average values are −0.41‰ ± 0.10‰ ($n = 6$), −0.37‰ ± 0.15‰ ($n = 4$), and − 0.16‰ ± 0.07‰ ($n = 3$). $\delta^{88}Sr$ values increase slightly upward through the section until the Hangenberg Shale, where they show a modest decrease. This pattern is consistent with trends observed in the three most abundant genera individually as well as with the overall LOESS function (Fig. 5). Throughout the entire section, *Branmehla* consistently exhibits lower $\delta^{88}Sr$ values than *Bispathodus* and *Palmatolepis*.

Residuals (*i.e.*, $\Delta^{88}Sr$) were calculated for each monospecific sample starting from the LOESS function (span = 0.75). These data provide $\delta^{88}Sr$ values "corrected" for the section stratigraphic trend, allowing us to evaluate differences among genera without the influence of eventual seawater fluctuations through time. The resulting $\Delta^{88}Sr$ values are: 0.10‰ ± 0.08‰ for *Palmatolepis*, 0.09‰ ± 0.09‰ for *Bispathodus*, −0.14‰ ± 0.11‰ for *Branmehla*, −0.10‰ ± 0.12‰ for *Mehlina*, −0.09‰ ± 0.17‰ for *Idioprioniodus* and 0.09 ± 0.07 for *Pandorinellina*. A Kruskal-Wallis test performed on $\Delta^{88}Sr$ shows significant differences among the six studied genera (Kruskal-Wallis rank sum $\chi^2 = 45.49$, $p = 1.1e\text{-}08$). *Post hoc* Dunn tests indicate significant differences between *Branmehla* and the two major genera, *Palmatolepis* (Z = 5.34; *p* adjusted = 1.3e-06) and *Bispathodus* (Z = −5.41; *p* adjusted = 9.3e-07). A significant difference is also observed between *Mehlina* and *Palmatolepis* (Z = 3.08; *p adjusted* = 0.025) and between *Bispathodus* and *Mehlina* (Z = −3.10, *p* adjusted = 0.025). Differences among other genus pairs are not statistically significant, although this may reflect the smaller sample sizes available for *Mehlina*, *Pandorinellina*, and *Idioprioniodus*.

Radiogenic Sr isotopes are reported and discussed stratigraphically by Letulle et al. (2025) for the main genera and here briefly summarised. The average $^{87}Sr/^{86}Sr$ values for the main genera *Palmatolepis*, *Bispathodus*, and *Branmehla* are 0.70829 ± 0.00004 (SD, $n = 22$), 0.70826 ± 0.00005 ($n = 23$), and 0.70827 ± 0.00005 ($n = 24$), respectively. For *Mehlina*, *Idioprioniodus*, and *Pandorinellina*, the averages are 0.70826 ± 0.00005 ($n = 6$), 0.70820 ± 0.00006 ($n = 4$), and 0.70821 ± 0.00001 ($n = 3$). Similarly to the $\delta^{88}Sr$, we calculated the $^{87}Sr/^{86}Sr$ residuals (*i.e.*, $\Delta^{87}Sr/^{86}Sr$) from a LOESS trend to highlight those values that deviates mostly from the general $^{87}Sr/^{86}Sr$ evolution. Such values can be considered somehow those that most likely underwent potential diagenetic alterations. The resulting $\Delta^{87}Sr/^{86}Sr$ values are as follows: 0.00001 ± 0.00002 for *Palmatolepis*, −0.00001 ± 0.00002 for *Bispathodus*, 0.00000 ± 0.00002 for *Branmehla*, 0.00000 ± 0.00003 for *Mehlina*, −0.00003 ± 0.00001 for *Idioprioniodus* and 0.00000 ± 0.00001 for *Pandorinellina*. A Kruskal-Wallis test performed on $\Delta^{87}Sr/^{86}Sr$ shows significant differences among the six studied genera (Kruskal-Wallis rank sum $\chi^2 = 16.93$, $p = 0.005$). Yet, *post hoc* Dunn tests indicate that significant differences exist only between *Idioprioniodus* and *Palmatolepis* (Z = 3.60, *p* adjusted = 0.005).

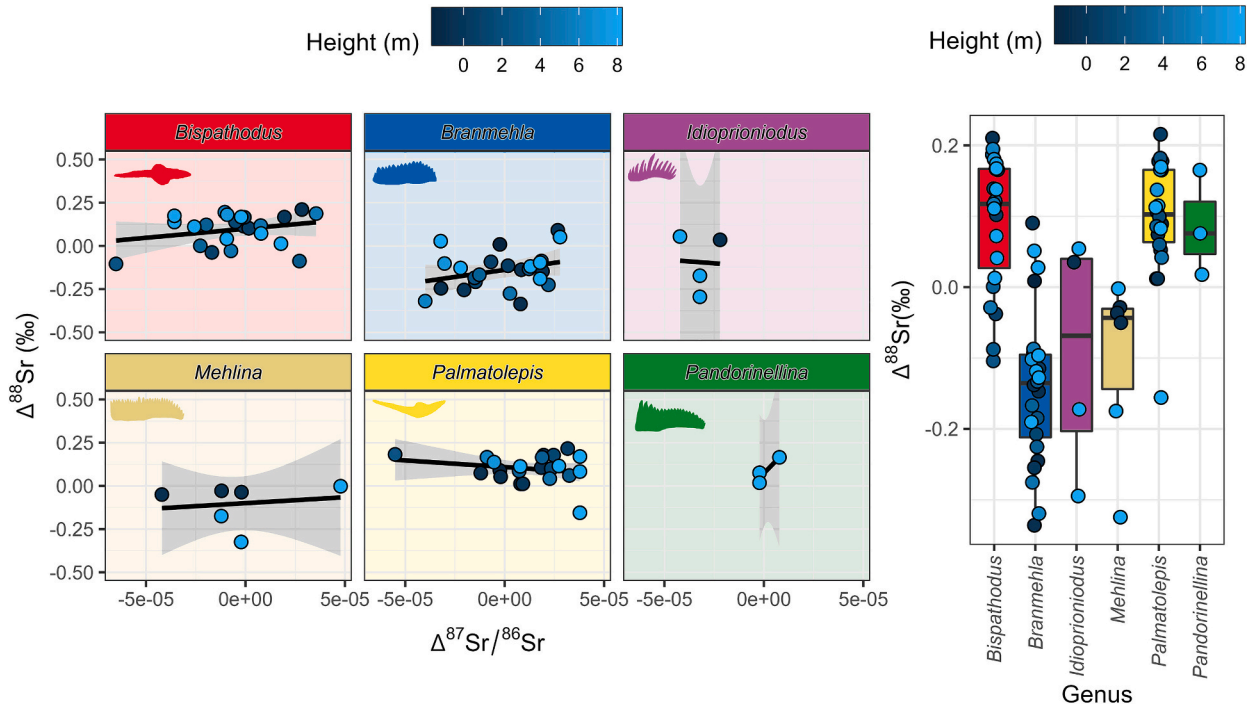

Fig. 7. Linear relationships between $\Delta^{88}Sr$ and $\Delta^{87}Sr/^{86}Sr$ residuals. No statistically significant correlations were observed. Boxplots of $\Delta^{88}Sr$ are also reported for each genus. Individual symbols are colored based on the samples' section height.

No statistically significant relationship has been found for $\Delta^{88}Sr$ *vs* $\Delta^{87}Sr/^{86}Sr$ (Fig. 7). Linear regressions of the six genera for $\Delta^{88}Sr$ *vs* $\Delta^{87}Sr/^{86}Sr$ provided the following results: $R^2 = 0.04$ ($p = 0.36$) for *Palmatolepis*, $R^2 = 0.07$ ($p = 0.23$) for *Bispathodus*, $R^2 = 0.09$ ($p = 0.14$) for *Branmehla*, $R^2 = 0.03$ ($p = 0.76$) for *Mehlina*, $R^2 = 0.00$ ($p = 0.96$) for *Idioprioniodus* and $R^2 = 0.85$ ($p = 0.26$) for *Pandorinellina.*

The results obtained by X-ray microdiffraction are reported in Table 1 and Table SM-2. The bioapatite cell size is mainly influenced by the presence of carbon element in the tetrahedral sites of the apatite framework of conodonts: the greater the amount of carbon, the lower the *a* parameter and slightly higher the *c* parameter; thus the *a/c* ratio is able to synthesize and emphasize inverse relations with respect to carbon content. No significant differences in unit-cell parameters (*a/c*) were observed among the main genera (Kruskal-Wallis rank sum $\chi^2 = 0.416$, $p = 0.812$), nor among the different areas of the element (Kruskal-Wallis rank sum $\chi^2 = 0.176$, $p = 0.674$). This indicates that any alteration of the apatite crystal structure is not measurably different across taxa.

Ca/P (wt%) ratios measured by ESEM-EDS (Table SM-3) show an average value of 2.26 ± 0.13 (1SD), while F content (wt%) an average of 4.3% ± 1.5% (1SD). No statistical differences were observed among genera for either Ca/P (Kruskal-Wallis rank sum $\chi^2 = 3.50$, $p = 0.32$) or F content (Kruskal-Wallis rank sum $\chi^2 = 6.71$, $p = 0.08$). Both Ca/P and F content resemble modern shark fluorapatite composition (Enax et al., 2012) and agree with reported well-preserved conodont fluorapatite (*e.g.*, Zhuravlev and Shevchuk, 2017; Zhuravlev and Smoleva, 2018; Zhuravlev, 2021; Terrill et al., 2022).

6. Discussion

6.1. Diagenetic alteration

Conodont crowns and their enamel-like tissue are among the skeletal tissues least affected by diagenesis (Trotter et al., 2007), eventually different between lamellar (hyaline) tissue and white matter (Trotter and Eggins, 2006; Griffin et al., 2021). We speculate that the observed differences in stable Sr isotopes between taxa may reflect variation in the proportion of white matter (albid tissue), a porous, non-permeable component of the conodont crown (Donoghue, 1998), likely more susceptible to diagenetic alteration (Trotter and Eggins, 2006). Differences among taxa in the relative amounts of white matter and lamellar (hyaline) tissue could therefore influence the bulk Sr signal. Yet, white-matter content has not been quantified for the taxa examined here, except for some *Palmatolepis* species (Müller and Nogami, 1971). If denticle number is taken as a rough proxy, *Palmatolepis*, with a large platform, might be expected to have relatively little white matter, whereas *Bispathodus*, with fused denticles forming most of the oral surface, might have more. Other blade-like elements would likely fall between these extremes. This pattern does not match our stable Sr results, as *Palmatolepis* shows values comparable to *Bispathodus*,

Table 1
X-ray microdiffraction data for the different taxa; unit cell parameters (*a*, *c* and the cell volume V) are reported as ranges and mean values (standard deviation in brackets).

Taxon	investigated area	*a* (Å), range	*a* (Å), mean	*c* (Å), range	*c* (Å), mean	V (Å^3), range	V (Å^3), mean
Branmehla	planar surface	9.358–9.374	9.369(5)	6.861–6.892	6.883(7)	520.8–524.4	523.2(9)
Branmehla	denticles	9.333–9.374	9.365(9)	6.865–6.919	6.885(16)	518.2–526.1	523.0(19)
Palmatolepis	planar surface	9.359–9.375	9.366(5)	6.877–6.910	6.887(8)	521.9–524.1	523.2(5)
Palmatolepis	denticles	9.340–9.384	9.367(10)	6.869–6.889	6.882(7)	519.0–525.0	522.9(15)
Bispathodus	planar surface	9.361–9.375	9.367(4)	6.854–6.900	6.885(11)	521.3–524.4	523.2(8)
Bispathodus	denticles	9.354–9.374	9.366(7)	6.869–6.904	6.883(8)	521.4–524.5	522.9(10)

supporting the idea that our Sr isotope data primarily reflect a biogenic signal and are not influenced by variations of white-matter proportions.

As mentioned above, all conodont elements used in this study exhibit a CAI value of 1.5, suggesting that they did not experience elevated temperatures or high-pressure conditions during diagenesis. Although some studies have proposed that conodont apatite may be altered even at low CAI values (Ebneth et al., 1997), additional evidence indicates that the Kowala material is generally well preserved. Our ESEM and X-ray microdiffraction data show no significant differences among the investigated genera. Moreover, the Ca/P ratio and F content are, on average, indistinguishable from modern shark fluorapatite, arguing against a chemical diagenetic overprint. Raman spectroscopy of the $\nu 1\text{-}PO_4^{3-}$ band performed on the crown tissue of *Palmatolepis gracilis* from Kowala (bed Ko-404, also analysed in this study; Fig. 5), compared to a large compilation of fossil bioapatites (Shirley et al., 2024), yields highly consistent peak positions. These data match values reported for well-preserved fossil apatites across diverse taxa and diagenetic settings. In addition, Letulle et al. (2025) showed that the $^{87}Sr/^{86}Sr$ range of Kowala conodonts is comparable to that of well-preserved Devonian-Carboniferous calcitic brachiopods from Royseux, Belgium (Azmy et al., 2009), and distinct from diagenetically altered conodonts from the Rhenish Slate Mountains (Kurschner et al., 1993). The decreasing trend observed at the base of the *Siphonodella* (*Eosiphonodella*) *praesulcata* Zone at Kowala is consistent with trends previously reported from well-preserved calcite brachiopods from the Rhenish Slate Mountains (Kurschner et al., 1993; Brand et al., 2004). Collectively, these results suggest that diagenesis exerted only a minor influence and that Sr in the Kowala conodonts is likely of biogenic origin.

Residuals of both $\delta^{88}Sr$ and $^{87}Sr/^{86}Sr$ for the three main genera do not show patterns consistent with alteration along the section. Specifically, the lack of correlation between $\Delta^{88}Sr$ *vs* $\Delta^{87}Sr/^{86}Sr$ argues against a common diagenetic overprint and makes it unlikely that diagenesis explains the observed variability. If diagenesis had significantly affected the samples, we would expect deviant $^{87}Sr/^{86}Sr$ values (Letulle et al., 2025) to be accompanied by coherent shifts in $\Delta^{88}Sr$, which are not observed. Moreover, sample height within the section shows no relationship with the magnitude of residuals per genus. Recent studies on vertebrate bioapatite show that in terrestrial settings (Armaroli et al., 2025; Michailow et al., 2025), diagenetic alteration tends to shift $\delta^{88}Sr$ values toward more positive compositions than typical biogenic signatures (~ −0.20‰), approaching a local diagenetic endmember that is often enriched in ^{88}Sr (*e.g.*, soil carbonates). In contrast, our data display, on average, ^{88}Sr-depleted values (−0.27‰), akin to the bioapatite of modern terrestrial vertebrates, but lighter than that of modern marine vertebrates (~0.10‰ of elasmobranchs; Le Houedec et al., 2017). This evidence advocates against a diagenetic alteration that -for what is known so far- should shift $\delta^{88}Sr$ toward heavier carbonate or terrigenous endmembers (see Wu et al., 2024), a trend not seen in our specimens.

Taken together, these lines of evidence suggest no significant diagenetic modification of our samples. No crystallinity disturbances, elemental anomalies, or isotopic trends indicative of alteration were detected. While a minor overprint cannot be entirely excluded, particularly given the limited constraints on how diagenesis affects conodont bioapatite chemistry, our results support the interpretation that the observed $\delta^{88}Sr$ variations primarily reflect biological signals rather than diagenetic alteration.

6.2. Vital effect?

Multiple factors can influence isotope ratios in animal biomineralised tissues, including dietary preferences, physiology, mobility, habitat, phylogenetic distance and behaviour. In terrestrial vertebrates, $\delta^{88}Sr$ has so far been associated mainly with diet and/or digestive physiology (Armaroli et al., 2025; Michailow et al., 2025; Weber et al., 2025). Given this context, the simplest explanation for our results is that co-occurring conodont genera occupied different trophic niches. The idea that conodonts partitioned ecological niches is well established (*e.g.*, Girard and Renaud, 2008, 2012; Ginot and Goudemand, 2019; Renaud et al., 2021), especially given that morphological diversity of elements in the oral apparatus, as well as their rapid evolution, appear to have been driven by selective pressures related to food processing (Nicoll, 1987; Świś, 2023; Shirley et al., 2024; Nesme et al., 2025). Recent studies combining morphology and geochemistry increasingly support trophic differentiation in conodonts (Zhuravlev, 2020; Zhuravlev et al., 2020; Terrill et al., 2022; Assemat et al., 2023). Accordingly, a difference in trophic level among the studied genera offer a likely explanation for the variation we detect in $\delta^{88}Sr$. In particular, we observe a $\Delta^{88}Sr$ between *Branmhela* and *Palmatolepis* (*i.e.*, $\delta^{88}Sr_{Branmehla}$ - $\delta^{88}Sr_{Palmatolepis}$) of ~0.27‰ ± 0.15‰ which is consistent with the reported trophic spacing in terrestrial vertebrate bioapatite ~ −0.20‰

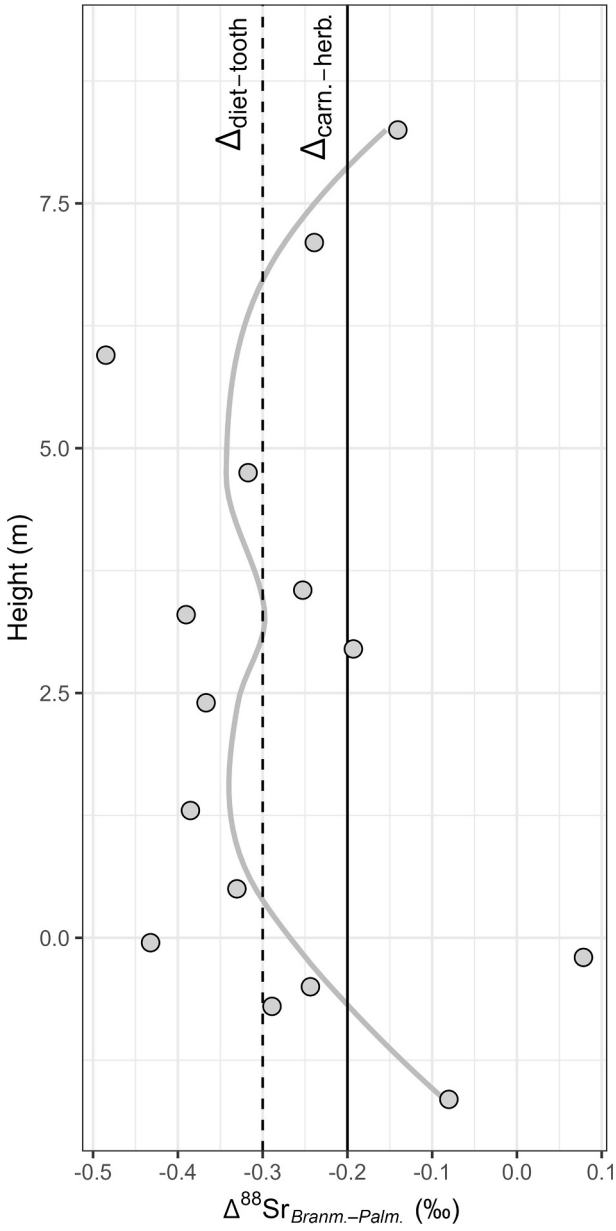

Fig. 8. Difference $\Delta^{88}Sr_{Branm.\text{-}Palm.}$ (*i.e.*, $\delta^{88}Sr_{Branmehla}$ - $\delta^{88}Sr_{Palmatolepis}$) between *Branmhela* and *Palmatolepis* isotope ratios across the Kowala section. The grey line is a LOESS smoothing function. The solid vertical line represents the expected trophic shift between carnivores and herbivore enamel (~ −0.20‰). The dashed line is the expected diet-bone discrimination factor (~ −0.30‰).

and a diet-bone discrimination of ~ −0.30‰ (Tütken et al., 2015; Guiserix et al., 2022, 2024; Dodat et al., 2025; Weber et al., 2025) (Fig. 8).

Our study focused on six distinct conodont apparatuses, each selected to represent a broad range of taxonomic diversity. These apparatuses include P_1 elements that correspond to three principal morphological categories, encompassing variations in platform architecture, denticulation patterns, and basal cavity development. This selection ensures coverage of the major structural designs observed within the Late Devonian conodont fauna, providing a robust basis for comparative analysis. The apparatus that stands out the most in our dataset is that of *Palmatolepis*, represented here by the monospecific late member *P. gracilis*. Its M elements possess elongated both anterior and posterior processes, a unique feature among our taxa. The S-series is light-looking and "spiky", with relatively short elements except for S_{3-4}. The S_0 is short and diadem-shaped. The P_2 is uniquely triramous, and the P_1 is the only platform-bearing element in the dataset. Platform-bearing P_1 elements show "molarization", in which an expanded surface forms between the basal cavity and the carina (in rostral and caudal view). The platform expands the element in the oral and aboral side and ranges from dorsal to base of free blade (see Fig. 2).

By contrast, the remaining genera possess the standard polygnathid-type apparatus with hook-like M elements with caudal process elongated and rot-like straight S-series. *Bispathodus* is the most robust and bears icrion-bearing P_1 elements; icrionization represents another form of molarization in which the carina becomes thickened into a working surface. *Pandorinellina* has a similar apparatus but a blade-like P_1 with a broadened basal cavity. *Branmehla* possesses a more delicate apparatus with a triangular S_1 and a blade-like P_1 with variable basal cavity expansion. *Mehlina* has a similar organization but with a narrow, highly denticulated blade-like P_1. *Idioprioniodus* uniquely combines a relatively delicate, lightly built P_1 with thick denticles widely spaced along the rest of the apparatus.

The $\delta^{88}Sr$ data separates the genera into two distinct clusters: *Palmatolepis*, *Bispathodus*, and *Pandorinellina* in one group, and *Branmehla*, *Mehlina*, and *Idioprioniodus* in the other. Previous studies have shown a trophic influence on stable Sr isotope compositions, with higher trophic level animals generally exhibiting lower $\delta^{88}Sr$ values (Knudson et al., 2010; Guiserix et al., 2022, 2024). This pattern likely reflects differences in dietary sources and associated physiological fractionation, suggesting that $\delta^{88}Sr$ signatures can serve as proxies for reconstructing feeding strategies and ecological niches within Late Devonian marine ecosystems. Applied to our material, this suggests that *Branmehla*, *Mehlina*, and *Idioprioniodus* occupied a higher trophic level than *Palmatolepis*, *Bispathodus*, and *Pandorinellina*. Based on apparatus morphology, the platform-bearing *Palmatolepis* might be expected to differ most strongly from the others due to its numerous unique modifications like slender appearance of S-series and triramous P_2 element. However, its $\delta^{88}Sr$ values are instead similar to those of the icrion-bearing *Bispathodus* and the blade-like *Pandorinellina*. By contrast, all taxa in the higher-trophic group share blade-like P_1 elements, whereas differences in the S-series, such as the robust denticles of *Idioprioniodus* or the distinctive S_1 of *Branmehla*, do not appear related to $\delta^{88}Sr$. Thus, in this dataset, P_1 morphology appears to be the strongest predictor of trophic position. Platform (in *Palmatolepis*), icrion (in *Bispathodus*) and possibly an expanded basal cavity (in *Pandorinellina*) are each associated with lower trophic levels, whereas fully blade-like P_1 elements (*Branmehla*, *Mehlina*, *Idioprioniodus*) correspond to higher trophic levels.

This is consistent with geochemical evidence (Sr-Ba/Ca) on Silurian conodonts (Terrill et al., 2018), where taxa with narrow-bladed P_1 elements (*Wurmiella excavata*, *Oulodus excavatus*) were inferred to occupy higher trophic positions than blade-like taxa with broader basal cavities (*Ozarkodina bohemica*, *Zieglerodina remscheidensis*) (Terrill et al., 2018). Biomechanical modelling of *Wurmiella* P_1 elements further shows that their sharp, blade-like denticles differ functionally from icrion-bearing taxa such as *Idiognathodus*, or blade-like taxa with broader basal cavities such as *Vogelgnathus campbelli* (Jones et al., 2012). Similar differences can be observed between *Palmatolepis*, *Bispathodus* and *Branmehla* in topographic metrics such as slope and Relief Index (RFI), which reflect element sharpness (Assemat et al., 2023). It should be noted here that the values of RFI of *Pandorinellina* were similar to blade-like elements in Assemat et al. (2023), work that is in contradiction to results presented here. This discrepancy could be the result of a different methodological approach of morphological study or regional variability between the Kowala and Montagne Noire populations.

At present, the only $\delta^{88}Sr$ data available for Devonian conodonts are from Le Houedec et al. (2017), with values ranging from −0.15‰ (similar to our *Palmatolepis* group) to −0.35‰ (closer to our *Branmhela* group) and a $\Delta^{88}Sr$ between the two of −0.20‰ (~ expected trophic shift); however, no genus-level information was reported. The same study reports Ca isotope ($\delta^{44/40}Ca_{915a}$) values of 0.04‰ and 0.07‰ for those samples, indistinguishable within uncertainty. This suggests that, assuming diagenesis is negligible, the physiological mechanism driving Ca and Sr isotope fractionations are eventually different or partially decoupled (see, *e.g.*, reptiles in Weber et al., 2025). In this sense, Balter et al. (2019) found no significant $\delta^{44/42}Ca$ differences among conodont taxa (in agreement with carbon isotope data from, *e.g.*, Zhuravlev and Smoleva, 2018; Zhuravlev, 2023), although the investigated genera were all platform- or icrion-bearing (*Ancyrodella*, *Ancyrognathus*, *Icriodus*, *Palmatolepis*, *Polygnathus*). Novel research on Ca and Sr isotope metabolism in the body supports this hypothesis. Box-modelling and physiological studies on Ca isotopes suggest that fractionation mainly occurs during bone mineralization and urine excretion (Eisenhauer et al., 2019; Tacail et al., 2020). Indeed, Ca isotopes along the trophic chain mainly reflect bone ingestion by carnivores (Martin et al., 2015; Dodat et al., 2024, 2025) and milk consumption (*e.g.*, Reynard et al., 2011; Hassler et al., 2021; Tacail et al., 2021). However, these interpretations rely on (limited) vertebrate data only and may not be directly transferable to organisms with distinct biological and physiological features. Notably, conodonts have no modern analogue, limiting direct comparisons with any modern taxa. The main mechanism guiding $\delta^{88}Sr$ isotope fractionation likely occurs in the gut. No modelling or experimental studies are available so far: however, some context can be inferred from current literature. For example, Armaroli et al. (2025) demonstrated that different digestive physiologies, rather than diet, might drive the observed $\delta^{88}Sr$ variability among herbivore foregut *vs* hindgut fermenters, possibly due to differences in, *e.g.*, gut retention time, ion transporters, or pH. This is also supported by the well-known Sr-over-Ca biopurification process (Burton et al., 1999), occurring along the trophic chain due to preferential gut excretion of Sr over Ca. Taken together, these patterns might suggest that $\delta^{88}Sr$ and $\delta^{44}Ca$ can record distinct ecological and physiological signals, with $\delta^{44}Ca$ mainly reflecting, *e.g.*, bone ingestion, while $\delta^{88}Sr$ more sensitive to the overall trophic position and digestive processing. Yet, the paucity of modern and fossil analog studies calls for cautiousness in interpreting these isotope patterns.

We cannot fully exclude that habitat partitioning and/or taxon-specific biomineralization pathways could have fractionated the $\delta^{88}Sr$ ratio of Kowala conodonts. Studies on calcifying marine organisms (such as coccolithophores and corals) indicate that light, temperature, salinity and Ca^{2+} transport mechanisms can directly or indirectly influence Sr metabolism, thereby altering both Sr/Ca ratios and $\delta^{88}Sr$ values (*e.g.*, Reynaud et al., 2004; Fietzke and Eisenhauer, 2006; Rüggeberg et al., 2008; Stevenson et al., 2014). However, extending these inferences to vertebrates such as conodonts is not straightforward, as their bioapatite-based tissues form through fundamentally different physiological and mineralization pathways than those of carbonate-producing organisms.

Future work should expand paleoecological studies of conodonts by integrating geochemical data (*i.e.*, multi-isotopes, trace elements) on well screened specimens and morphometrics to better separate environmental from biological signals. Building larger datasets across depositional settings and time will be essential to test whether the

isotopic offsets observed in our study are consistent or dependent on, *e.g.*, locality, event, or evolutionary trajectories. Finally, modern studies in living or recent fossil organisms with different diet and digestive physiology will be crucial to understand vertebrate geochemical patterns, allowing a robust reconstruction of trophic level and habitat use through deep time.

7. Conclusions

The $\delta^{88}Sr$ values of the Late Devonian conodont fauna from the Kowala section distinctly cluster the taxa into two discrete groups. Higher values are observed in *Palmatolepis*, *Bispathodus*, and *Pandorinellina*, whereas *Branmehla*, *Mehlina*, and *Idioprioniodus* record lower values. The crystallographic assessment of bioapatite and the absence of trends in either $^{87}Sr/^{86}Sr$ or $\delta^{88}Sr$, indicate that these patterns are unlikely to result from diagenetic alteration. Instead, the genus-dependent variability indicates that alteration is not uniform across taxa, emphasizing the need to avoid assuming equivalent reliability of all genera in isotope-based stratigraphic frameworks.

Recent studies link $\delta^{88}Sr$ values in vertebrate bioapatite to dietary differences and physiology, hinting to a similar biological origin for the variations observed in our conodonts. Moreover, the degree of $\delta^{88}Sr$ difference between our two groups is comparable to the value reported between trophic levels (*e.g.*, herbivores *vs* carnivores) in modern ecosystems (Guiserix et al., 2022, 2024; Weber et al., 2025), supporting the hypothesis that the two groups might represent different positions within the trophic network.

Finally, although differences in apparatus composition alone do not fully explain distinct feeding strategies, the morphology of the caudalmost P_1 element aligns well with the $\delta^{88}Sr$ groupings. Conodonts with blade-like P_1 elements (*Branmehla*, *Mehlina*, *Idioprioniodus*) fall within the lower $\delta^{88}Sr$ range, whereas taxa with surface structures P_1 elements like platform (*Palmatolepis*), icrion (*Bispathodus*), or those with enlarged basal cavities (*Pandorinellina*) exhibit higher values. This pattern suggests that, in general, conodonts with blade-like P_1 elements might have occupied higher trophic levels than those with more morphologically complex P_1 structures.

CRediT authorship contribution statement

Przemysław Lech Świś: Writing – original draft, Validation, Investigation, Formal analysis. **Annalisa Ferretti:** Writing – review & editing, Writing – original draft, Validation, Investigation, Funding acquisition, Conceptualization. **Manuel Rigo:** Writing – review & editing, Writing – original draft, Validation, Supervision, Investigation, Funding acquisition, Conceptualization. **Thomas Letulle:** Validation, Investigation, Formal analysis. **Anna Cipriani:** Writing – review & editing, Methodology. **Luca Medici:** Validation, Investigation, Formal analysis. **Daniele Malferrari:** Validation, Investigation, Formal analysis. **Federico Lugli:** Writing – original draft, Validation, Supervision, Investigation, Formal analysis, Conceptualization.

Declaration of competing interest

The authors declare the following financial interests/personal relationships which may be considered as potential competing interests:

Manuel Rigo reports financial support was provided by Italian Ministry of University and Research. Annalisa Ferretti reports financial support was provided by Italian Ministry of University and Research. If there are other authors, they declare that they have no known competing financial interests or personal relationships that could have appeared to influence the work reported in this paper.

Acknowledgements

This research was undertaken within the framework and with the financial support of the International Union of Geological Sciences (IUGS) and the European Community – Next Generation EU, Italian Ministry of University and Research, PRIN–PNRR 2022 Project P2022K9BE8, “OCEANS” granted to MR and AF.

Appendix A. Supplementary data

Supplementary data to this article can be found online at https://doi.org/10.1016/j.palaeo.2026.113755.

Data availability

The authors confirm that all data necessary for supporting the scientific findings of this paper have been provided.

References

Argentino, C., Lugli, F., Cipriani, A., Panieri, G., 2021. Testing miniaturized extraction chromatography protocols for combined $^{87}Sr/^{86}Sr$ and $\delta^{88}/^{86}Sr$ analyses of pore water by MC-ICP-MS. L&O Methods 19, 431–440.
Armaroli, E., Lugli, F., Cipriani, A., Tütken, T., 2024. Spatial ecology of moose in Sweden: Combined Sr-O-C isotope analyses of bone and antler. PLoS One 19, e0300867.
Armaroli, E., Cheheb, R.C., Cipriani, A., Bernardini, S., van der Made, J., Cáceres, I., Sahnouni, M., Lugli, F., 2025. Stable Sr isotopes of fossil dental enamel reflect diet and digestive system differences among sympatric herbivores. Palaeogeogr. Palaeoclimatol. Palaeoecol. 678, 113226.
Assemat, A., Thiery, G., Lieffroy, T., Girard, C., 2023. Shape diversity in conodont elements, a quantitative study using 3D topography. Mar. Micropaleontol. 184, 102292.
Azmy, K., Poty, E., Brand, U., 2009. High-resolution isotope stratigraphy of the Devonian-Carboniferous boundary in the Namur-Dinant Basin, Belgium. Sediment. Geol. 216, 117–124.
Balter, V., Martin, J.E., Tacail, T., Suan, G., Renaud, S., Girard, C., 2019. Calcium stable isotopes place Devonian conodonts as first level consumers. Geochem. Perspect. Lett. 10, 36–39.
Becker, R.T., Kaiser, S.I., Aretz, M., 2016. Review of chrono-, litho- and biostratigraphy across the global Hangenberg Crisis and Devonian-Carboniferous Boundary. Geol. Soc. Spec. Publ. 423, 355–386.
Becker, R.T., Marshall, J.E.A., Da Silva, A.-C., Agterberg, F.P., Gradstein, F.M., Ogg, J.G., 2020. The Devonian period. In: Gradstein, F., M., Ogg, J.G., Schmitz, M.D., Ogg, G. M. (Eds.), Geologic Time Scale 2020. Elsevier, pp. 733–810.
Becker, R.T., Hartenfels, S., Kaiser, S.I., 2021. Review of Devonian-Carboniferous Boundary sections in the Rhenish Slate Mountains (Germany). Palaeobiodivers. Paleoenviron. 101, 357–420.
Boogaard, M., Kuhry, B., 1979. Statistical reconstruction of the *Palmatolepis* apparatus (Late Devonian conodontophorids) at the generic, sub-generic, and specific level. Scr. Geol. 49, 1–57.
Brand, U., Legrand-Blain, M., Streel, M., 2004. Biochemostratigraphy of the Devonian-Carboniferous boundary global stratotype section and point, Griotte Formation, La Serre, Montagne Noire, France. Palaeogeogr. Palaeoclimatol. Palaeoecol. 205, 337–357.
Burton, J.H., Price, T.D., Middleton, W.D., 1999. Correlation of bone Ba/Ca and Sr/Ca due to biological purification of Calcium. J. Archaeol. Sci. 26, 609–616.
Corradini, C., Ferretti, A., Serpagli, E., 1998. The Silurian and Devonian sequence in SE Sardinia. Giorn. Geol. 60, 71–74.
Corradini, C., Henderson, C., Barrick, J.E., Ferretti, A., 2026. Conodonts in Biostratigraphy. A 300-million-years long journey through geologic time. Newsl. Stratigr. 59, 77–116.
De Vleeschouwer, D., Rakociński, M., Racki, G., Bond, D.P.G., Sobień, K., Claeys, P., 2013. The astronomical rhythm of Late-Devonian climate change (Kowala section, Holy Cross Mountains, Poland). Earth Planet. Sci. Lett. 365, 25–37.
Dodat, P.-J., Albalat, E., Balter, V., Couture-Veschambre, C., Hardy, M., Henrion, J., Holliday, T., Maureille, B., 2024. Diverse bone-calcium isotope compositions in Neandertals suggest different dietary strategies. J. Hum. Evol. 193, 103566.
Dodat, P.-J., Guiserix, D., Jaouen, K., Montes, L., Utrilla, P., Villalba-Mouco, V., Maureille, B., Balter, V., 2025. Enhancing the reconstruction of the Gabasa Neandertal's diet using Ca and Sr stable isotopes. J. Hum. Evol. 207, 103747.
Donoghue, P.C.J., 1998. Growth and patterning in the conodont skeleton. Philos. Trans. R. Soc. B Biol. Sci. 353, 633–666.
Du, Y., Chiari, M., Karádi, V., Nicora, A., Onoue, T., Pálfy, J., Roghi, G., Tomimatsu, Y., Rigo, M., 2020. The asynchronous disappearance of conodonts: new constraints from Triassic-Jurassic boundary sections in the Tethys and Panthalassa. Earth-Sci. Rev. 203, 103176.
Du, Y., Onoue, T., Karádi, V., Williams, I.S., Rigo, M., 2021. Evolutionary Process from *Mockina bidentata* to *Parvigondolella andrusovi*: Evidence from the Pizzo Mondello Section, Sicily, Italy. J. Earth Sci. 32, 667–676.
Du, Y., Onoue, T., Tomimatsu, Y., Wu, Q., Rigo, M., 2023. Lower Jurassic conodonts from the Inuyama area of Japan: implications for conodont extinction. Front. Ecol. Evol. 11, 1135789.

Dzik, J., 1991. Evolution of oral apparatuses in the conodont chordate. Acta Palaeontol. Pol. 36, 265–323.
Dzik, J., 2006. The Famennian "golden age" of conodonts and ammonoids in the Polish part of the Variscan sea. Palaeontol. Pol. 63, 1–360.
Dzik, J., 2008. Evolution of morphogenesis in 360-million-year-old conodont chordates calibrated in days. Evol. Dev. 10, 769–777.
Dzik, J., Phong, N.D., Thuy, N.T., Świś, P., 2022. Evolution and migration of conodonts and ammonoids near the end of Devonian recorded in distant localities. Stratigraphy 19, 27–50.
Ebneth, S., Diener, A., Buhl, D., Veizer, J., 1997. Strontium isotope systematics of conodonts: Middle Devonian, Eifel Mountains, Germany. Palaeogeogr. Palaeoclimatol. Palaeoecol. 132, 79–96.
Eisenhauer, A., Müller, M., Heuser, A., Kolevica, A., Glüer, C.C., Both, M., Laue, C., Hehn, U.V., Kloth, S., Shroff, R., Schrezenmeir, J., 2019. Calcium isotope ratios in blood and urine: A new biomarker for the diagnosis of osteoporosis. Bone Rep. 10, 100200.
Enax, J., Prymak, O., Raabe, D., Epple, M., 2012. Structure, composition, and mechanical properties of shark teeth. J. Struct. Biol. 178, 290–299.
Epstein, A.G., Epstein, J.B., Harris, L.D., 1977. Conodont color alteration - an index to organic metamorphism. USGS Prof. Pap. 995, 1–25.
Ferretti, A., Malferrari, D., Medici, L., Savioli, M., 2017. Diagenesis does not invent anything new: precise replication of conodont structures by secondary apatite. Sci. Rep. 7, 1624.
Ferretti, A., Bancroft, A.M., Repetski, J.E., 2020. GECkO: Global Events impacting COnodont evolution. Palaeogeogr. Palaeoclimatol. Palaeoecol. 549, 109677.
Ferretti, A., Medici, L., Savioli, M., Mascia, M.T., Malferrari, D., 2021. Dead, fossil or alive: bioapatite diagenesis and fossilization. Palaeogeogr. Palaeoclimatol. Palaeoecol. 579, 110608.
Ferretti, A., Corradini, C., Fakir, S., Malferrari, D., Medici, L., 2023. To be or not to be a conodont. The controversial story of *Pseudooneotodus* and *Eurytholia*. Mar. Micropaleontol. 182, 102258.
Fietzke, J., Eisenhauer, A., 2006. Determination of temperature-dependent stable strontium isotope ($^{88}Sr/^{86}Sr$) fractionation via bracketing standard MC-ICP-MS. Geochem. Geophys. Geosyst. 7, Q08009.
Foote, M., Sepkoski, J.J., 1999. Absolute measures of the completeness of the fossil record. Nature 398, 415–417.
Ginot, S., Goudemand, N., 2019. Conodont size, trophic level, and the evolution of platform elements. Paleobiology 45, 458–468.
Girard, C., Renaud, S., 2008. Disentangling allometry and response to Kellwasser anoxic events in the late Devonian conodont genus Ancyrodella. Lethaia 41, 383–394.
Girard, C., Renaud, S., 2012. Disparity changes in 370 Ma Devonian fossils: The signature of ecological dynamics? PLoS One 7, e36230.
Goudemez, C., Assemat, A., Thiery, G., Girard, C., 2026. 3D topography as an indicator of change in food processing ability in elements of the conodont genus *Palmatolepis*. Lethaia 59, 1–16.
Griffin, J.M., Montañez, I.P., Glessner, J.J.G., Chen, J., Willmes, M., 2021. Geologic variability of conodont strontium isotopic composition quantified by laser ablation multiple collection inductively coupled plasma mass spectrometry. Palaeogeogr. Palaeoclimatol. Palaeoecol. 568, 110308.
Guiserix, D., Albalat, E., Ueckermann, H., Davechand, P., Iaccheri, L.M., Bybee, G., Badenhorst, S., Balter, V., 2022. Simultaneous analysis of stable and radiogenic strontium isotopes in reference materials, plants and modern tooth enamel. Chem. Geol. 606, 121000.
Guiserix, D., Dodat, P.J., Jaouen, K., Albalat, E., Mendes Cardoso, J., Maureille, B., Balter, V., 2024. Stable isotope composition and concentration systematics of Ca and trace elements (Zn, Sr) in single aliquots of fossil bone and enamel. Geochim. Cosmochim. Acta 367, 123–132.
Hassler, A., Martin, J.E., Ferchaud, S., Grivault, D., Le Goff, S., Albalat, E., Hernandez, J. A., Tacail, T., Balter, V., 2021. Lactation and gestation controls on calcium isotopic compositions in a mammalian model. Metallomics 13, mfab019.
Henderson, C.M., 2020. Subchapter 3D – Conodonts. In: Gradstein, F.M., Ogg, J.G., Schmitz, M.D., Ogg, G.M. (Eds.), Geologic Time Scale 2020. Elsevier, pp. 56–60.
Holland, T.J.B., Redfern, S.A.T., 1997. Unit cell refinement from powder diffraction data: the use of regression diagnostics. Mineral. Mag. 61, 65–77.
House, M.R., 2002. Strength, timing, setting and cause of mid-Palaeozoic extinctions. Palaeogeogr. Palaeoclimatol. Palaeoecol. 181, 5–25.
Joachimski, M.M., Buggisch, W., 2002. Conodont apatite $\delta^{18}O$ signatures indicate climatic cooling as a trigger of the Late Devonian mass extinction. Geology 30, 711–714.
Jones, D., Evans, A.R., Siu, K.K.W., Rayfield, E.J., Donoghue, P.C.J., 2012. The sharpest tools in the box? Quantitative analysis of conodont element functional morphology. Proc. R. Soc. B Biol. Sci. 279, 2849–2854.
Kaiser, S.I., 2009. The Devonian/Carboniferous boundary stratotype section (La Serre, France) revisited. Newsl. Stratigr. 43, 195–205.
Kaiser, S.I., Aretz, M., Becker, R.T., 2016. The global Hangenberg Crisis (Devonian-Carboniferous transition): review of a first-order mass extinction. Geol. Soc. Spec. Publ. 423, 387–437.
Kelz, V., Guenser, P., Rigo, M., Jarochowska, E., 2023. Growth allometry and dental topography in Upper Triassic conodonts support trophic differentiation and molar-like element function. Paleobiology 5, 665–683.
Knudson, K.J., Williams, H.M., Buikstra, J.E., Tomczak, P.D., Gordon, G.W., Anbar, A.D., 2010. Introducing $\delta^{88}/^{86}Sr$ analysis in archaeology: A demonstration of the utility of strontium isotope fractionation in paleodietary studies. J. Archaeol. Sci. 37, 2352–2364.
Korte, C., Kozur, H.W., Bruckschen, P., Veizer, J., 2003. Strontium isotope evolution of late Permian and Triassic seawater. Geochim. Cosmochim. Acta 67, 47–62.
Krystyn, L., 2010. Decision report on the defining event for the base of the Rhaetian stage. Albertiana 38, 11–12.
Kurschner, W., Becker, R.T., Buhl, D., Veizer, J., 1993. Strontium isotopes in conodonts: Devonian-Carboniferous transition, the northern Rhenish Slate Mountains, Germany. Ann. Soc Géol. Belg. 115, 595–621.
Le Houedec, S., McCulloch, M., Trotter, J., Rankenburg, K., 2017. Conodont apatite $\delta^{88}/^{86}Sr$ and $\delta^{44}/^{40}Ca$ compositions and implications for the evolution of Palaeozoic to early Mesozoic seawater. Chem. Geol. 453, 55–65.
Letulle, T., Świś, P.L., Lugli, F., Ferretti, A., Rigo, M., 2025. Conodont apatite record of marine Sr isotopic composition in the advent of the Hangenberg Event (Late Devonian). Chem. Geol. 692, 122981.
Lewis, J., Pike, A.W.G., Coath, C.D., Evershed, R.P., 2017. Strontium concentration, radiogenic ($^{87}Sr/^{86}Sr$) and stable ($\delta^{88}Sr$) strontium isotope systematics in a controlled feeding study. Sci. Technol. Archaeol. Res. 3, 45–57.
Liu, H.P., Bergström, S.M., Witzke, B.J., Briggs, D.E.G., McKay, R.M., Ferretti, A., 2017. Exceptionally preserved conodont apparatuses with giant elements from the Middle Ordovician Winneshiek Konservat-Lagerstätte, Iowa, USA. J. Paleontol. 91, 493–511.
Malec, J., 2014. The Devonian/Carboniferous boundary in the Holy Cross Mountains (Poland). Geol. Q. 58, 217–234.
Malferrari, D., Ferretti, A., Mascia, M.T., Savioli, M., Medici, L., 2019. How much can we trust major element quantification in bioapatite investigation? ACS Omega 4, 17814–17822.
Malferrari, D., Ferretti, A., Medici, L., 2024. The origin and significance of euhedral apatite crystals on conodonts. Mar. Micropaleontol. 186, 102308.
Martin, J.E., Tacail, T., Adnet, S., Girard, C., Balter, V., 2015. Calcium isotopes reveal the trophic position of extant and fossil elasmobranchs. Chem. Geol. 415, 118–125.
Marynowski, L., Zatoń, M., Rakociński, M., Filipiak, P., Kurkiewicz, S., Pearce, T.J., 2012. Deciphering the upper Famennian Hangenberg Black Shale depositional environments based on multi-proxy record. Palaeogeogr. Palaeoclimatol. Palaeoecol. 346–347, 66–86.
Matyja, H., Woroncowa-Marcinowska, T., Filipiak, P., Brański, P., Sobień, K., 2021. The Devonian/Carboniferous boundary interval in Poland: multidisciplinary studies in pelagic (Holy Cross Mountains and Sudetes) and ramp (Western Pomerania) successions. Palaeobiodivers. Paleoenviron. 101, 421–472.
McArthur, J.M., Howarth, R.J., Shields, G.A., Zhou, Y., 2020. Chapter 7 - Strontium isotope stratigraphy. In: Gradstein, F.M., Ogg, J.G., Schmitz, M.D., Ogg, G.M. (Eds.), Geologic Time Scale 2020. Elsevier, pp. 211–238.
Medici, L., Malferrari, D., Savioli, M., Ferretti, A., 2020. Mineralogy and crystallization patterns in conodont bioapatite from first occurrence (Cambrian) to extinction (end-Triassic). Palaeogeogr. Palaeoclimatol. Palaeoecol. 549, 109098.
Medici, L., Savioli, M., Ferretti, A., Malferrari, D., 2021. Zooming in REE and other trace elements on conodonts: Does taxonomy guide diagenesis? J. Earth Sci. 32, 501–511.
Medici, L., Ferretti, A., Collareta, A., Bosio, G., Bianucci, G., Carnevale, G., Casati, S., Clò, S., Lanteri, L., Lugli, F., Marramà, G., Mollen, F.H., Savioli, M., Malferrari, D., 2026. Bioapatite crystallinity and Rare Earth Element signatures in fossil and Recent sharks: A window into Past and Present seas. Chem. Geol. 702, 123200.
Michailow, M.M., Lugli, F., Cipriani, A., Della Giustina, F., Ferretti, A., Malferrari, D., Fowler, D., Fowler, E.F., Weber, M., Tütken, T., 2025. Combined Ca, Sr isotope and trace element analyses of Late Cretaceous dinosaur teeth: assessing diet *versus* diagenesis. Geochim. Cosmochim. Acta 400, 172–189.
Müller, K.J., Nogami, Y., 1971. Über den Feinbau der Conodonten. Mem. Fac. Sci. Kyoto Univ. Ser. Geol. Mineral. 38, 1–109.
Murdock, D.J.E., Dong, X.P., Repetski, J.E., Marone, F., Stampanoni, M., Donoghue, P.C. J., 2013. The origin of conodonts and of vertebrate mineralized skeletons. Nature 502, 546–549.
Myrow, P.M., Ramezani, J., Hanson, A.E., Bowring, S.A., Racki, G., Rakociński, M., 2014. High-precision U-Pb age and duration of the latest Devonian (Famennian) Hangenberg Event, and its implications. Terra Nova 26, 222–229.
Nesme, F., Girard, C., Joachimski, M.M., Corradini, C., Cornée, J.-J., Renaud, S., 2025. Geometric morphometrics suggests different environmental pressures on small and large *Polygnathus* conodonts during the recovery after the Hangenberg crisis (latest Devonian – earliest Carboniferous). Palaeontology 68, e70033.
Nicoll, R.S., 1987. Form and function of the Pa element in the conodont animal. In: Aldridge, R.J. (Ed.), Palaeobiology of Conodonts. Ellis Hardwood, Chichester, pp. 77–90.
Onoue, T., Yamashita, K., Fukuda, C., Soda, K., Tomimatsu, Y., Abate, B., Rigo, M., 2018. Sr isotope variations in the Upper Triassic succession at Pizzo Mondello, Sicily: constraints on the timing of the Cimmerian Orogeny. Palaeogeogr. Palaeoclimatol. Palaeoecol. 499, 131–137.
Pisarzowska, A., Rakociński, M., Marynowski, L., Szczerba, M., Thoby, M., Paszkowski, M., Perri, M.C., Spalletta, C., Schönlaub, H.P., Kowalik, N., Gereke, M., 2020. Large environmental disturbances caused by magmatic activity during the Late Devonian Hangenberg Crisis. Glob. Planet. Chang. 190, 103155.
Pisarzowska, A., Mariusz, P., Kołtonik, K., Budzyń, B., Szczerba, M., Rakociński, M., Sláma, J., Anna, Z., Łaptaś, A., 2022. Geotectonic settings of Variscan explosive volcanism in the light of Famennian tuffites provenance from southern Poland. Earth-Sci. Rev. 234, 104218.
Purnell, M.A., Donoghue, P.C.J., Aldridge, R.J., 2000. Orientation and anatomical notation in conodonts. J. Paleontol. 74, 113–122.
Racki, G., 1993. Evolution of the bank to reef complex in the Devonian of the Holy Cross Mountains. Acta Palaeontol. Pol. 37, 87–182.
Renaud, S., Girard, C., Dufour, A.B., 2021. Morphometric variance, evolutionary constraints and their change through time in Late Devonian *Palmatolepis* conodonts. Evolution 75, 2911–2929.

Reynard, L.M., Henderson, G.M., Hedges, R.E.M., 2011. Calcium isotopes in archaeological bones and their relationship to dairy consumption. J. Archaeol. Sci. 38, 657–664.
Reynaud, S., Ferrier-Pagès, C., Boisson, F., Allemand, D., Fairbanks, R.G., 2004. Effect of light and temperature on calcification and strontium uptake in the scleractinian coral *Acropora verweyi*. Mar. Ecol. Prog. Ser. 279, 105–112.
Rigo, M., Joachimski, M.M., 2010. Palaeoecology of Late Triassic conodonts: constraints from oxygen isotopes in biogenic apatite. Acta Palaeontol. Pol. 55, 471–478.
Rigo, M., Trotter, J.A., Preto, N., Williams, I.S., 2012. Oxygen isotopic evidence for Late Triassic monsoonal upwelling in the northwestern Tethys. Geology 40, 515–518.
Rigo, M., Bertinelli, A., Concheri, G., Gattolin, G., Godfrey, L., Katz, M.E., Maron, M., Mietto, P., Muttoni, G., Sprovieri, M., Stellin, F., Zaffani, M., 2016. The Pignola-Abriola section (southern Apennines, Italy): a new GSSP candidate for the base of the Rhaetian Stage. Lethaia 49, 287–306.
Romaniello, S.J., Field, M.P., Smith, H.B., Gordon, G.W., Kim, M.H., Anbar, A.D., 2015. Fully automated chromatographic purification of Sr and Ca for isotopic analysis. JAAS 30, 1906–1912.
Rüggeberg, A., Fietzke, J., Liebetrau, V., Eisenhauer, A., Dullo, W.C., Freiwald, A., 2008. Stable strontium isotopes ($\delta^{88}/^{86}$Sr) in cold-water corals - A new proxy for reconstruction of intermediate ocean water temperatures. Earth Planet. Sci. Lett. 269, 570–575.
Sansom, I.J., Smith, M.P., Armstrong, H.A., Smith, M.M., 1992. Presence of the earliest vertebrate hard tissues in conodonts. Science 256, 1308–1311.
Schönlaub, H.P., Corradini, C., Corriga, M.G., Ferretti, A., 2017. Chrono-, litho- and conodont bio-stratigraphy of the Rauchkofel Boden section (Upper Ordovician-Lower Devonian), Carnic Alps, Austria. Newsl. Stratigr. 50, 445–469.
Shirley, B., Grohganz, M., Bestmann, M., Jarochowska, E., 2018. Wear, tear and systematic repair: testing models of growth dynamics in conodonts with high-resolution imaging. Proc. R. Soc. B Biol. Sci. 285, 20181614.
Shirley, B., Leonhard, I., Murdock, D.J.E., Repetski, J., Świś, P., Bestmann, M., Trimby, P., Ohl, M., Plümper, O., King, H.E., Jarochowska, E., 2024. Increasing control over biomineralization in conodont evolution. Nat. Commun. 15, 5273.
Stevenson, E.I., Hermoso, M., Rickaby, R.E.M., Tyler, J.J., Minoletti, F., Parkinson, I.J., Mokadem, F., Burton, K.W., 2014. Controls on stable strontium isotope fractionation in coccolithophores with implications for the marine Sr cycle. Geochim. Cosmochim. Acta 128, 225–235.
Świś, P., 2023. Anagenetic evolution and peramorphosis of a latest Devonian conodont from Holy Cross Mountain (Poland). J. Micropalaeontol. 42, 193–210.
Szulczewski, M., Skompski, S., 1995. Ostrówka. In: Dvořák, J., Galle, A., Herbig, H.G., Krejči, Z., Malec, J., Paszkowski, M., Racki, G., Skompski, S., Szulczewski, M., Żakowa, H. (Eds.), XIII International Congress on Carboniferous–Permian, August 28–September 2, 1995, Kraków, Poland. Guide to Excursion B4: Evolution of the Polish-Moravian Carbonate Platform in the Late Devonian and Early Carboniferous: Holy Cross Mts., Kraków Upland. M. Polish Geological Institute, Warsaw.
Tacail, T., Le Houedec, S., Skulan, J.L., 2020. New frontiers in calcium stable isotope geochemistry: perspectives in present and past vertebrate biology. Chem. Geol. 537, 119471.
Tacail, T., Martin, J.E., Herrscher, E., Albalat, E., Verna, C., Ramirez-Rozzi, F., Clark, G., Valentin, F., Balter, V., 2021. Quantifying the evolution of animal dairy intake in humans using calcium isotopes. Quat. Sci. Rev. 256, 106843.
Terrill, D.F., Henderson, C.M., Anderson, J.S., 2018. New applications of spectroscopy techniques reveal phylogenetically significant soft tissue residue in Paleozoic conodonts. J. Anal. At. Spectrom. 33, 992.
Terrill, D.F., Jarochowska, E., Henderson, C.M., Shirley, B., Bremer, O., 2022. Sr/Ca and Ba/Ca ratios support trophic partitioning within a Silurian conodont community from Gotland, Sweden. Paleobiology 48, 601–621.
Trotter, J.A., Eggins, S.M., 2006. Chemical systematics of conodont apatite determined by laser ablation ICPMS. Chem. Geol. 233, 196–216.
Trotter, J.A., Fitz Gerald, J.D., Kokkonen, H., Barnes, C.R., 2007. New insights into the ultrastructure, permeability, and integrity of conodont apatite determined by transmission electron microscopy. Lethaia 40, 97–110.
Trotter, J.A., Williams, I.S., Nicora, A., Mazza, M., Rigo, M., 2015. Long-term cycles of Triassic climate change: A new δ^{18}O record from conodont apatite. Earth Planet. Sci. Lett. 415, 165–174.
Tütken, T., Held, P., Herrmann, S., Galer, S., 2015. Combined $\delta^{88}/^{86}$Sr and ^{87}Sr/^{86}Sr in bones and teeth: a toolbox for diet and habitat reconstruction. In: 25th Anniversary of the Goldschmidt Conference, Prague, 16th-21st August, p. 3196. Abstract.
Veizer, J., Ala, D., Azmy, K., Bruckschen, P., Buhl, D., Bruhn, F., Garden, G.A.F., Diener, A., Ebneth, S., Godderis, Y., Jasper, T., Korte, C., Pawellek, F., Podlaha, O.G., Strauss, H., 1999. ^{87}Sr/^{86}Sr, δ^{13}C and δ^{18}O evolution of Phanerozoic seawater. Chem. Geol. 161, 59–88.
Vollstaedt, H., Eisenhauer, A., Wallmann, K., Böhm, F., Fietzke, J., Liebetrau, V., Krabbenhöft, A., Farkaš, J., Tomašových, A., Raddatz, J., Veizer, J., 2014. The Phanerozoic $\delta^{88}/^{86}$Sr record of seawater: new constraints on past changes in oceanic carbonate fluxes. Geochim. Cosmochim. Acta 128, 249–265.
Weber, J., Bracco, J.N., Poplawsky, J.D., Ievlev, A.V., More, K.L., Lorenz, M., Bertagni, A. L., Jindra, S.A., Starchenko, V., Higgins, S.R., Stack, A.G., 2018. Unraveling the Effects of Strontium Incorporation on Barite Growth - In Situ and Ex Situ Observations Using Multiscale Chemical Imaging. Cryst. Growth Des. 18, 5521–5533.
Weber, M., Weber, K., Winkler, D.E., Tütken, T., 2025. Calcium and strontium isotopes in extant diapsid reptiles reflect dietary tendencies—a reference frame for diet reconstructions in the fossil record. Proc. R. Soc. B Biol. Sci. 292, 20242002.
Wu, N., Zhang, J., Mao, H., Zhang, G., Zhao, Z., 2024. Geochemical behavior of stable strontium isotopes during continental weathering process: a review. Geosyst. Geoenviron. 3, 100144.
Zhuravlev, A.V., 2020. Trophic position of some Late Devonian-Carboniferous (Mississippian) conodonts revealed on carbon organic matter isotope signatures: a case study of the East European basin. Geodiversitas 42, 443–453.
Zhuravlev, A.V., 2021. Middle-Late Paleozoic conodont ecogeochemistry: an overview. Vestn. Geosci. 3, 31–34.
Zhuravlev, A.V., 2023. Carbon isotope study of conodont elements: applications and limitations. Mar. Micropaleontol. 178, 102200.
Zhuravlev, A.V., Shevchuk, S.S., 2017. Strontium distribution in upper devonian conodont elements: a palaeobiological proxy. Riv. Ital. Paleontol. Stratigr. 123, 203–210.
Zhuravlev, A.V., Smoleva, I.V., 2018. Carbon isotope values in conodont elements from the latest Devonian–Early carboniferous carbonate platform facies (Timan-Pechora Basin). Est. J. Earth Sci. 67, 238–246.
Zhuravlev, A.V., Plotitsyn, A.N., Gruzdev, D.A., 2020. Carbon Isotope Ratios in the Apatite-Protein Composites of Conodont Elements—Palaeobiological Proxy. In: Lecture Notes in Earth System Sciences, pp. 749–764.